

Direct observation of charge-density waves in $\text{Ho}_5\text{Ir}_4\text{Si}_{10}$

C. M. Tseng,¹ C. H. Chen,^{1,2,3,*} and H. D. Yang⁴

¹Center for Condensed Matter Sciences, National Taiwan University, Taipei 10617, Taiwan

²Department of Physics, National Taiwan University, Taipei 10617, Taiwan

³Institute of Atomic and Molecular Sciences, Academia Sinica, Taipei 10617, Taiwan

⁴Department of Physics, Center of Nanoscience and Nanotechnology, National Sun-Yat-Sen University, Kaohsiung 80424, Taiwan

(Received 20 March 2008; published 30 April 2008)

We report the direct observation of charge-density waves in $\text{Ho}_5\text{Ir}_4\text{Si}_{10}$ by dark-field imaging in transmission electron microscopy using superlattice diffraction spots. The incommensurate phase of charge-density wave is found to be discommensurate with small commensurate domains separated by domain walls (discommensurations). Configurations of charge-density wave dislocations convincingly show that the charge-density wave phase transition is accompanied by a concomitant cell-doubling crystallographic structural phase transition, an unprecedented phenomenon in other charge-density wave systems.

DOI: [10.1103/PhysRevB.77.155131](https://doi.org/10.1103/PhysRevB.77.155131)

PACS number(s): 71.45.Lr, 64.70.Rh, 61.44.Fw, 61.05.jm

I. INTRODUCTION

Despite its seemingly three-dimensional crystallographic structure, the tetragonal rare-earth transition-metal silicide system, $R_5T_4\text{Si}_{10}$, where $R=\text{Dy}$, Ho , Er , Tm , and Lu , and $T=\text{Ir}$ and Rh , has been shown to exhibit fascinating charge-density wave (CDW) phase transitions,¹⁻¹¹ a phenomenon found largely in low-dimensional systems, which exhibit increased nested portions of anisotropic Fermi surfaces favorable for CDW formations. Due to lack of band structure calculations for the $R_5T_4\text{Si}_{10}$ system, it is still unclear why the seemingly three-dimensional structure would facilitate the formation of CDWs. Although it is generally thought that the rare-earth ions in the particular $R1$ positions of the crystal seem to form quasi-one-dimensional chains,^{3,4} which lead to a CDW instability, the spacing of the rare-earth ions (4.2 Å) along the “chains” seems too large to be considered as one dimensional. The unexpected presence of CDW phase transitions in this class of materials has drawn much attention in recent years. Thermal and electrical transport measurements have all clearly demonstrated two anomalies in the temperature range of $40\text{ K} < T < 200\text{ K}$, which were interpreted to be normal to incommensurate and incommensurate to commensurate CDW phase transitions.^{1,2,5,7,8} The crucial x-ray diffraction evidences for the CDW transitions have also been demonstrated in single crystals,^{3,4,9} which show the appearance of satellite superlattice peaks.

The most unusual characteristic of the CDW transition revealed by x-ray diffraction in the $R_5T_4\text{Si}_{10}$ system was the observation that commensurate superlattice peaks at cell-doubling positions along the c axis were found to simultaneously appear with the incommensurate CDW satellites with $q=(0,0,1/4 \pm \delta)$ when cooled from the normal state.^{4,9} The concomitant occurrence of the commensurate superlattice reflections with the incommensurate CDW modulations, unprecedented in CDW transitions, was conjecturally interpreted as a structural phase transition with cell doubling, which facilitates the CDW formation by modifications of the Fermi surface.⁴ Electronic phase transitions driven by concomitant crystallographic structural transitions have drawn much attention recently in view of the new finding that the

enigmatic Verwey transition in magnetite is actually caused by a gap opening in the electronic band structure due to the simultaneous crystal-structural phase transformation to a lower symmetry phase.¹² The implications of this proposition in our case, if true, will likewise give rise to new thinking of the CDW formation in the presence of new Fermi surface topology, newly added phonon modes, and new landscapes of electron phonon coupling, which plays the critical roles for all CDW transitions. It is, therefore, of great importance to firmly establish the nexus of the structural phase transition and the CDW characteristics. Furthermore, with lack of band structure information in this class of materials, appearance of satellite reflections besides the anomalies observed in transport and thermal measurements does not automatically attest to the correctness of the CDW's interpretation. Information obtained from real space observations should also be able to produce additional evidence to verify the generally accepted exposition.

In this paper, we report important findings for the CDW phase transitions in $\text{Ho}_5\text{Ir}_4\text{Si}_{10}$ by electron diffraction and direct observation in real space using satellite dark-field imaging technique in transmission electron microscopy (TEM). The real space images obtained from the satellite reflections associated with the CDW phase transitions clearly demonstrated that the CDW incommensurate phase should be accurately described as discommensurate with small commensurate domains separated by sharp domain walls [discommensurations (DCs)] where the phase of CDW modulations changes rapidly. Examinations of the configuration of DCs further reveal the presence of CDW dislocations, which convincingly show that a crystallographic cell-doubling lattice distortion indeed occurs simultaneously with the CDW phase transition.⁴

II. EXPERIMENT

The preparation and characterization of the polycrystalline samples of $\text{Ho}_5\text{Ir}_4\text{Si}_{10}$ have been described elsewhere.¹ Thin specimens for TEM studies were prepared by mechanical polishing followed by ion milling at liquid nitrogen temperature. Our experiments were carried out in five different

grains from two different samples using a JEOL 2000 FX transmission electron microscope operating at 200 kV and equipped with a low temperature sample stage and a 14 bit charge-coupled-device imaging detector. The transport properties of these bulk samples before thinning for TEM studies were already reported.^{1,8} All the experimental results discussed in our paper are totally reproducible with the transition temperatures that fall within 3 K from different runs.

III. RESULTS AND DISCUSSIONS

TEM examinations show that a typical grain size is larger than a few micrometers, which can be treated as single crystals in the present case since selected area electron diffraction patterns require only an area much smaller than $1 \mu\text{m}$ in size. Electron diffraction studies at room temperature confirm the known tetragonal structure. The electron diffraction evidence of the CDW formation in $\text{Ho}_5\text{Ir}_4\text{Si}_{10}$ is shown in Figs. 1(a) and 1(b), which represent the $[010]$ zone-axis electron diffraction patterns taken at temperatures of 146 and 81 K, respectively. Sharp satellite spots not present at room temperature are evident in addition to the fundamental Bragg reflections. The transition temperatures for the normal to incommensurate and the incommensurate to commensurate phase transitions are determined in our experiments to be ~ 165 and 97 K, respectively, consistent with the x-ray diffraction results.⁹ It should be noted that the spurious forbidden fundamental Bragg reflections at the systematic $(h 0 l)$ positions with $h=\text{odd}$ and $l=\text{all integers}$, already present at room temperature, appear as a result of dynamical multiple scattering and should be ignored. The CDW modulation wave vectors can be deduced from Fig. 1(a) as $q_-(0, 0, 1/4 - \delta)$ and $q_+(0, 0, 1/4 + \delta)$ where $\delta \sim 0.025$ is the incommensurability. As the temperature is further lowered, the incommensurate CDW locks into a commensurate state with $\delta=0$, as shown in Fig. 1(b) where the doublet incommensurate satellite spots collapse into a single spot with $q=(0, 0, 1/4)$. The measurement of incommensurability δ as a function of temperature is also shown in Fig. 1(c) and the incommensurate to lock-in (commensurate) transition is found to take place at 97 K, which is ~ 20 K lower than that from the transport and thermal measurements in arc-melted samples.⁸ Some fluctuations of transition temperatures have been noted among the arc-melted samples.¹³ It is interesting to note from Fig. 2(c) that the peak width of commensurate satellite is much broader than that of the incommensurate ones. The same effect can also be seen from the x-ray data of $\text{Er}_5\text{Ir}_4\text{Si}_{10}$.⁴ We believe that the presence of significant residual strains in the commensurate phase could be responsible for this effect. In addition to the incommensurate peaks, from Figs. 1(a) and 1(b), new commensurate superlattice peaks located at systematic positions $(h 0 1/2)$ with $h=\text{all integers}$ were also simultaneously observed with the presence of the incommensurate satellites and the commensurate superlattice peaks persisted down to temperatures in the commensurate phase.⁴ The new commensurate superlattice peaks are characterized by a wave vector $q=(0, 0, 1/2)$. If the commensurate superlattice peaks of $(h, 0, 1/2)$ are interpreted as new fundamental Bragg peaks due to a structural

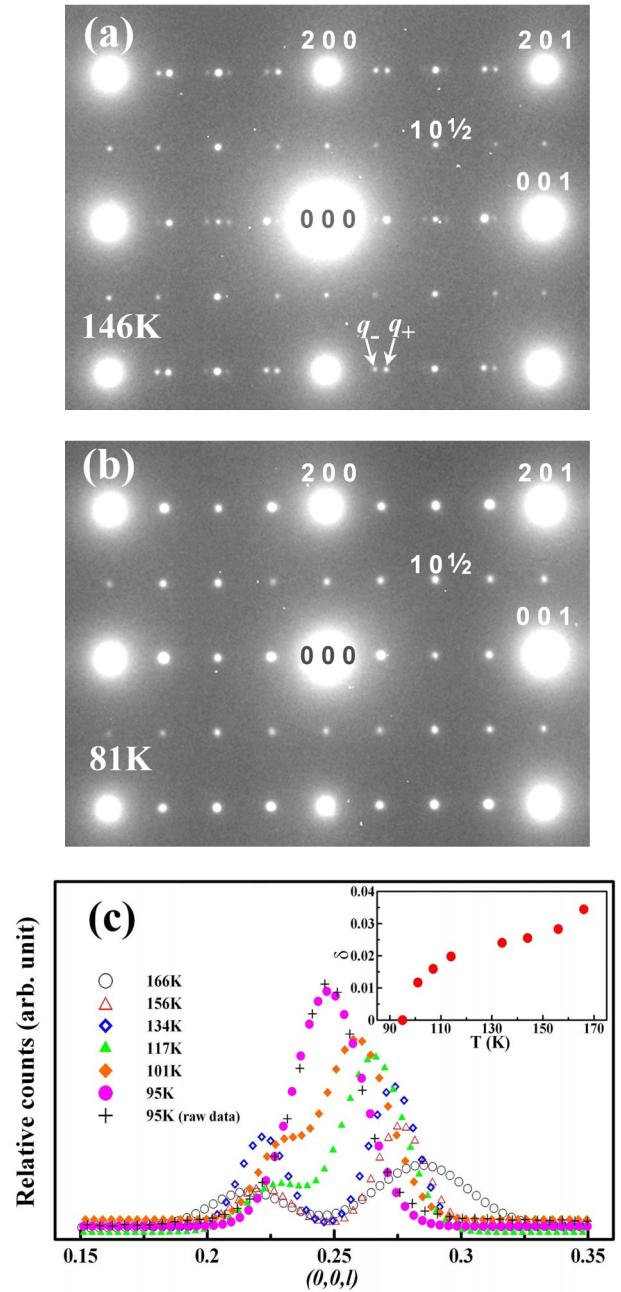


FIG. 1. (Color online) (a) Electron diffraction pattern along the $[010]$ zone axis obtained at 146 K, which shows the incommensurate satellite spots of charge-density wave modulations. The satellite reflections around $(0, 0, 0.5)$ peak arise from the artifacts of multiple reflections and should be ignored. (b) The same electron diffraction pattern obtained at 81 K, which shows the commensurate satellite peaks. (c) Gaussian fitted intensity scans of the satellite peaks along $(00l)$ at various temperatures, which show the incommensurate to commensurate transition. Raw data for the 95 K profile are also shown. The inset depicts the change of incommensurability δ as a function of temperature.

phase transition involving a cell-doubling along the c axis, then the doublet incommensurate satellite modulation wave vectors can be reduced to a single one with $q_+(0, 0, 1/4 + \delta)$ or $q_-(0, 0, 1/4 - \delta)$ since the satellite peaks can now be consistently referred from the commensurate peaks at the

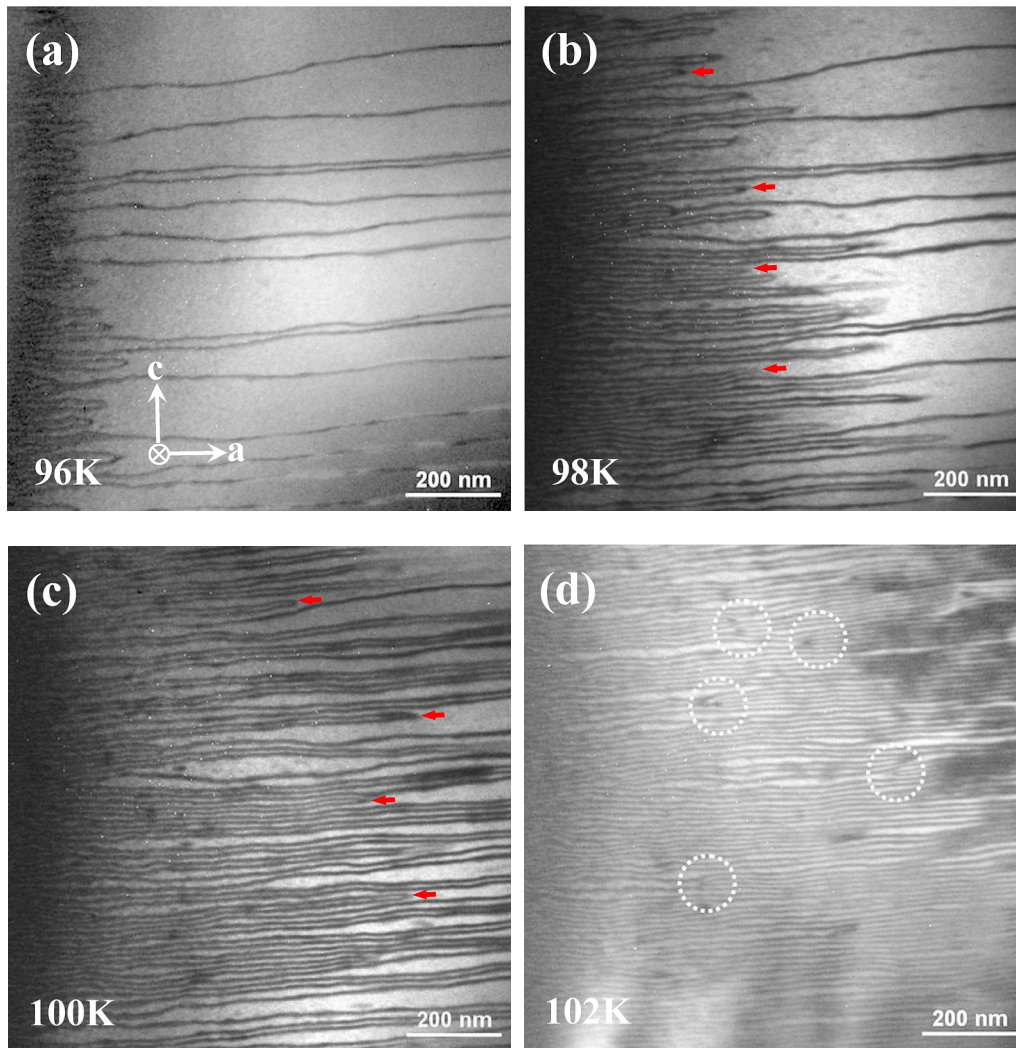


FIG. 2. (Color online) Superlattice dark-field images taken at various temperatures from the same area, which show the residual domain walls (discommensurations) in the commensurate phase (a) and the presence and movement of charge-density wave dislocations in (b)–(d). All the images were taken from the satellite peaks located at $(4, 0, 1/4 \pm \delta)$. It is noted that two discommensurations are always required to form a charge-density wave dislocation. A few corresponding dislocations marked by arrows in (b) and (c) seem to move at a slower speed than others. Some of the newly nucleated charge-density wave dislocations are marked with circles in (d).

systematic $(h, 0, 1/2)$ (with $h = \text{even}$) reflections and the neighboring fundamental Bragg peaks. Satellite peaks closest to the fundamental peaks are generally taken to characterize the modulation wave vectors and $q_- = (0, 0, 1/4 - \delta)$ would be the CDW wave vector under this scenario.⁴ However, we note that the intensity of the q_+ satellites is generally much higher than the q_- ones, and the asymmetry of the satellite doublet is anomalous for typical satellite modulations centered around $q = (0, 0, 1/4)$. Moreover, for satellites associated with the systematic weak $(h, 0, 1/2)$ reflections with $h = \text{odd}$, only q_+ satellites are detected with appreciable intensity. It is known that intensities of superlattice satellites usually follow that of the nearest fundamental lattice Bragg reflections they are associated with. The disparity of intensity between the weaker q_- and stronger q_+ satellites as shown in Fig. 1(a) can now be understood accordingly if q_- satellites are ascribed to the weaker cell-doubling superlattice peaks $(h, 0, 1/2)$ (with $h = \text{even}$) and the q_+ satellites to the much stronger fundamental Bragg peaks. Under these consider-

ations, we conclude that the incommensurate CDW should be described by a single modulation wave vector q_+ , which can then be written as $q_{CDW} = (0, 0, 1/2 + 2\delta)$ under the nomenclature of the new structure with cell-doubling along the c axis.

We now turn to the direct observation of CDW domains and domain walls using the satellite dark-field real space imaging method in TEM. This rather unique and powerful imaging technique has been shown to reveal the most direct details and the dynamics of CDW phase transitions.^{14–18} Figure 2 shows a series of dark-field images obtained from the CDW satellite peaks at several different temperatures near the commensurate to incommensurate CDW transition on warming. The most striking feature of the dark-field images is the presence of few slightly wavy dark lines largely perpendicular to the c axis (and parallel to the a axis). These lines, in fact, are planes extended through the thickness of sample (~ 50 nm) and seen as lines in projection parallel to the incident electron beam. These dark lines signify the ex-

istence of domain walls, also known as DCs, in the CDW state where rapid phase changes take place and the regions with lighter contrast between the DCs are commensurate CDW domains accordingly. An incommensurate modulation characterized by the presence of commensurate domains separated by DCs has been known as a discommensurate phase.¹⁹ Below the lock-in temperature in the commensurate phase, sparse residual DCs due to pinning can still be seen in Fig. 2(a) taken at 96 K despite the null incommensurability δ suggested from the electron diffraction pattern [Fig. 1(b)]. A much higher density of DCs, in fact, exists in the thinner area near the thinner edge of the sample [left-hand side of Fig. 2(a)], which signifies the strong pinning of DCs at the sample edge. As the temperature is raised slightly, shown in Fig. 2(b) obtained at 98 K, these pinned DCs near the thin edge start to move and spread out into the thicker areas of sparsely populated DCs. Close examination of the dynamics of the DCs reveals that the motion of the DCs is led by nodes where two DCs are joined together forming the so-called CDW dislocations.^{14,15,19} Many CDW dislocations are evident in Fig. 2(b). It is well known that the number of DCs required to form a CDW dislocation is determined by the commensurability order n of a CDW modulation wave vector $q=(0,0,1/n)$. A phase change of $2\pi/n$ takes place across each DC and n DCs are required to constitute a CDW dislocation so that the total phase change around the dislocation is 2π . The fact that two DCs are always needed in the present case to form a CDW dislocation demonstrates that the phase shift across a DC is π and the modulation wave vector should be of the type $q=(0,0,1/2)$ instead of $q=(0,0,1/4)$, which would otherwise require four DCs to merge at a CDW dislocation node. The c -axis cell-doubling structural phase transition, which simultaneously occurs with CDW, would automatically lower the order of commensurability from $n=4$ to $n=2$ and, hence, requires only two DCs to form a CDW dislocation. The direct observation of CDW dislocations consisting of two DCs provides an elegant and convincing proof that the cell-doubling structural phase transformation does occur concomitantly with CDW, an unprecedented phenomenon in CDW transitions with far-reaching implications. We note that a crystal-structural transformation to lower symmetry phase has been identified very recently as the driving force for the outstanding Verwey transition in magnetite,¹² which has puzzled the physics community for more than 60 years.

The CDW dislocations continue to move along the a -axis direction into the thicker area as the temperature is again increased, which results in further lengthening of DCs. Figures 2(c) and 2(d) display images taken at 100 and 102 K, respectively. CDW dislocations are found to move with different speeds, which reflect the local pinning strength fluctuations along the path they encounter. A few CDW dislocations, marked by arrows in Fig. 2(b), seem to move much slower than others and still visible in Fig. 2(c). It is noted that the original residual DCs observed at lower temperatures in the thicker area as shown in Fig. 2(a) remain largely motionless and unchanged in the initial warming process, which signifies the strong pinning effect of the CDWs. Pinning of CDWs is of considerable importance for the transport properties of CDW systems and has been treated in numerous

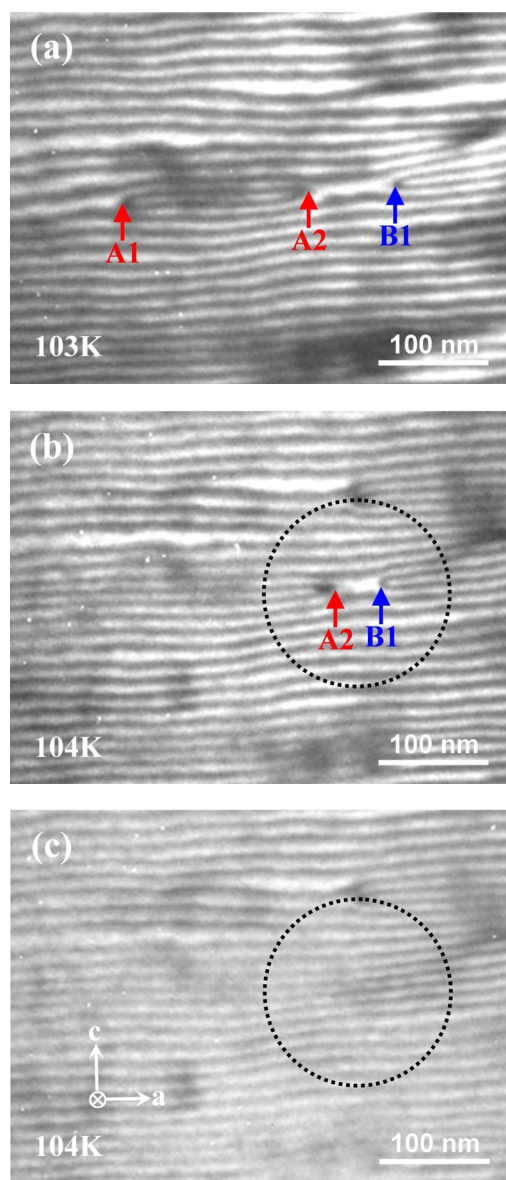


FIG. 3. (Color online) (a) Enlarged dark-field images (taken at ~ 103 K), which show the presence of an isolated charge-density wave dislocation dipole A with an adjacent dipole B. The nodes of the charge-density wave dislocations are marked as A1, A2, and B1 (B2 is outside the picture and not shown). As the temperature is slightly increased, A2 and B1 move closer (b) and eventually annihilate each other and disappear when they meet (c).

theoretical studies.^{20–22} It is generally believed that impurities and crystalline defects predominantly act as pinning centers for CDWs. No extended crystalline defects, such as dislocations and stacking faults, are visible in Fig. 2 and this leaves impurities and point defects, which are not visible in typical TEM studies, as possible pinning centers in the present case. This observation is consistent with the recent experimental finding that atomic disorder has significant effects on the CDW phase transitions in the $R_5T_4Si_{10}$ system.⁸

In addition to the motion of original CDW dislocations, nucleation of new CDW dislocations at higher temperatures can also be seen in Figs. 2(c) and 2(d), which results in an increasing density of DCs and gives rise to a larger incom-

measurability δ . It is noted that nucleation of CDW dislocations always occurs in pair, a node and an antinode, which forms a dislocation dipole. Some of the newly nucleated CDW dislocations squeezed in the space between DCs are marked in Fig. 2(d). A single isolated CDW dislocation dipole marked with two nodes as A1 and A2, however, was actually captured during the warming process, shown in Fig. 3(a), with another CDW dislocation marked as B1 in close proximity. At a slightly higher temperature, CDW dislocations A2 and B1 moved closer to each other [Fig. 3(b)] and were eventually annihilated forming continuous DCs [Fig. 3(c)]. The dynamics of the commensurate to incommensurate phase transition is entirely controlled by the process of nucleation, growth, and annihilation of the CDW dislocations. Through our studies, the edge of samples and grain boundaries are found to have a strong pinning effect for the CDW dislocations. However, nucleation, growth, and motion of the CDW dislocations are largely unimpeded within the crystal grains.

IV. CONCLUSIONS

In conclusion, dark-field images obtained from $\text{Ho}_5\text{Ir}_4\text{Si}_{10}$ CDW satellite peaks show ordered array of commensurate

domains separated by domain walls (discommensurations) in the incommensurate phase, which should be more accurately described as discommensurate accordingly.¹⁹ Configurations of CDW dislocations, where two (instead of four) discommensurations are found to form a node, convincingly show that the CDW phase transition is accompanied by a concomitant cell-doubling structural phase transition, an unprecedented phenomenon in other CDW systems. Electron diffraction studies show that the CDW modulation wave vector in $\text{Ho}_5\text{Ir}_4\text{Si}_{10}$ is characterized by $q=(0,0,1/2+2\delta)$, consistent with the concomitant cell-doubling structural phase transition along the c axis.

ACKNOWLEDGMENTS

We thank Y. K. Kuo at National Tung-Hwa University for helpful discussions. The research at National Taiwan University and National Sun-Yat-Sen University is supported by the National Science Council of Taiwan, under Contract Nos. NSC95-2120-M002-016 and NSC95-2112-M110-023, respectively.

*Author to whom correspondence should be addressed; chchen35@ntu.edu.tw

¹H. D. Yang, P. Klavins, and R. N. Shelton, Phys. Rev. B **43**, 7688 (1991).

²K. Ghosh, S. Ramakrishnan, and G. Chandra, Phys. Rev. B **48**, 4152 (1993).

³B. Becker, N. G. Patil, S. Ramakrishnan, A. A. Menosvky, G. J. Nieuwenhuys, J. A. Mydosh, M. Kohgi, and K. Iwasa, Phys. Rev. B **59**, 7266 (1999).

⁴F. Galli, S. Ramakrishnan, T. Tanigushi, G. J. Nieuwenhuys, J. A. Mydosh, S. Geupel, J. Ludecke, and S. Van Smaalen, Phys. Rev. Lett. **85**, 158 (2000).

⁵Y. K. Kuo, C. S. Lue, F. H. Hsu, H. H. Li, and H. D. Yang, Phys. Rev. B **64**, 125124 (2001).

⁶C. S. Lue, F. H. Hsu, H. H. Li, H. D. Yang, and Y. K. Kuo, Physica C **364-365**, 243 (2001).

⁷C. S. Lue, Y. K. Kuo, F. H. Hsu, H. H. Li, H. D. Yang, P. S. Fodor, and L. E. Wenger, Phys. Rev. B **66**, 033101 (2002).

⁸Y. K. Kuo, F. H. Hsu, H. H. Li, H. L. Huang, C. W. Huang, C. S. Lue, and H. D. Yang, Phys. Rev. B **67**, 195101 (2003).

⁹S. van Smaalen, M. Shaz, L. Palatinus, P. Daniels, F. Galli, G. J. Nieuwenhuys, and J. A. Mydosh, Phys. Rev. B **69**, 014103 (2004).

¹⁰H. L. Liu, G. S. Wu, J. L. Her, and H. D. Yang, Phys. Rev. B **72**,

205102 (2005).

¹¹F. Bondino, E. Magnano, E. Carleschi, M. Zangrando, F. Galli, J. A. Mydosh, and F. Parmigiani, J. Phys.: Condens. Matter **18**, 5773 (2006).

¹²G. Kh. Rozenberg, M. P. Pasternak, W. Y. Xu, Y. Amiel, M. Hanfland, M. Amboage, R. D. Taylor, and R. Jeanloz, Phys. Rev. Lett. **96**, 045705 (2006).

¹³Y. K. Kuo (private communication).

¹⁴C. H. Chen, J. M. Gibson, and R. M. Fleming, Phys. Rev. Lett. **47**, 723 (1981).

¹⁵C. H. Chen, J. M. Gibson, and R. M. Fleming, Phys. Rev. B **26**, 184 (1982).

¹⁶K. K. Fung, S. McKernan, J. W. Steed, and J. A. Wilson, J. Phys. C **14**, 5417 (1981).

¹⁷C. H. Chen and R. M. Fleming, Phys. Rev. B **29**, 4811 (1984).

¹⁸Y. Koyama, Z. P. Zhang, and H. Sato, Phys. Rev. B **36**, 3701 (1987).

¹⁹W. L. McMillan, Phys. Rev. B **12**, 1187 (1975); **14**, 1496 (1976).

²⁰P. A. Lee and T. M. Rice, Phys. Rev. B **19**, 3970 (1979).

²¹H. Fukuyama and P. A. Lee, Phys. Rev. B **17**, 535 (1978).

²²T. M. Rice, S. Whitehouse, and P. Littlewood, Phys. Rev. B **24**, 2751 (1981).